

## Investigating the Physical Mechanisms of Blazar Emission: A Multi-Zone Emission Model

---

**Stella S. Boula**<sup>a,\*</sup>

<sup>a</sup>*Institute of Nuclear Physics Polish Academy of Sciences  
Radzikowskiego 152, PL-31342 Kraków, Poland*

*E-mail:* [stboula@ifj.edu.pl](mailto:stboula@ifj.edu.pl)

Blazars are a type of active galactic nuclei that exhibit highly variable, non-thermal emission across the electromagnetic spectrum. This study presents an expanding emission model to investigate the physical processes leading to the blazar multi-wavelength emission. We explore the role of external photon fields in producing their high-energy emission and study the particle acceleration timescale to model their flaring activity. We aim to investigate the correlations between the flux at different wavelengths to gain insight into the physical properties of these intriguing astrophysical objects.

38th International Cosmic Ray Conference (ICRC2023)  
26 July - 3 August, 2023  
Nagoya, Japan



---

\*Speaker

## 1. Introduction

Compact regions located at the center of galaxies, known as Active Galactic Nuclei (AGN), house supermassive black holes with masses ranging from  $10^6$  to  $10^{10}$  times that of our Sun. These regions efficiently convert their dynamic energy into radiation through mass accretion. The resulting photons span the entire electromagnetic spectrum, ranging from radio waves to  $\gamma$ -rays.

Blazars, a specific subgroup of AGN, exhibit distinct features, including powerful relativistic jets directed towards us. These blazars possess exceptional energy emission, display rapid fluctuations in luminosity, and emit non-thermal radiation characterized by a distinct  $\gamma$ -ray signature. Their unique spectra can only be explained by a population of highly charged ultra-relativistic particles, turning these sources into cosmic accelerators. Blazars are categorized into two primary subgroups: Flat Spectrum Radio Quasars (FSRQs) and BL Lac objects. FSRQs predominantly exhibit strong emission lines in their spectra and have higher overall bolometric luminosity than BL Lac objects.

Considering the existing theoretical models, it can be stated that these models are primarily based on the assumption that particles undergo high-energy acceleration within a specific region situated inside the jet [1]. Additionally, the emitted radiation results from the interaction between the accelerated charged particles, magnetic fields, and ambient photon fields in the acceleration region. Models that propose electrons as the radiating particles are called leptonic models and can effectively explain the observed spectra. However, relativistic protons within these sources cannot be ruled out, necessitating the study of models that consider both types of particles, known as lepto-hadronic models. The emitted particle spectrum is calculated using radiative transfer equations incorporating high-energy processes. Astrophysical environments with high energy densities in photon and magnetic fields pose particularly complex radiation production and propagation challenges. Addressing these challenges, an innovative numerical approach to the problem was introduced by [2] and later developed by [3]. These articles presented all the relevant physical interactions between relativistic protons, electrons, and photons, constructing self-consistent kinetic equations. The system consists of three interconnected integro-differential equations that describe the temporal and spectral evolution of the particles. This work primarily focuses on the leptonic scenario and its ability to provide insights into open questions regarding the localization of emission and rapid variability observed in blazars. One unresolved question pertains to the localization of radio emission in blazars [4]. It is well-established that relativistic electrons absorb low-frequency radio photons, resulting in a distinctive "break" in the spectrum at the synchrotron self-absorption frequency [5]. However, blazars display radio emissions that cannot be explained when modeling this emission alongside their emissions at other frequencies. Hence, a simple explanation could be that radio photons originate from a separate region along the jet.

We extend the numerical code to address this issue by incorporating the source's adiabatic expansion and particle acceleration [6, 7]. This expansion allows us to simulate the temporal evolution of high-energy electrons as they propagate along the jet. Consequently, the overall spectrum of these sources arises from the combination of various spectra emitted by individual regions within the jet. The flow transforms into a continuous conical jet, influenced by the boundary conditions at the jet's base and its dynamic behavior. By comparing our results with observations, we can identify radio emission's localization, and its characteristics, and unveil the properties of the

radiating relativistic electrons. We should mention that recently [8, 9] also discussed the expansion model in detail and studied the emission of these sources.

## 2. Numerical setup

We assume an emitting region (a blob of radiative relativistic electrons) that expands with an expanding velocity  $u_{\text{exp}}$ . The blob of plasma is assumed to be spherical with radius  $R(t) = R_0 + u_{\text{exp}}t$  in its co-moving frame (where  $R_0$  is the initial radius of the source). It moves with highly relativistic speed  $\beta c$ , giving it a Lorentz factor  $\Gamma = (1 - \beta^2)^{-1/2}$ . The jet makes an angle  $\theta$  to our line of sight; thus, the relativistic Doppler factor is  $\delta = [\Gamma(1 - \beta \cos \theta)]^{-1}$ . The magnetic field has the strength

$$B = B_0 \left( \frac{R_0}{R} \right)^s, \quad (1)$$

where  $B_0$  is the initial value of the magnetic field and  $s$  is a free parameter.

The broader morphology of the non-thermal Blazar SED depends on the ratio of the magnetic to photon energy densities. We assume the power of the accretion

$$P_{\text{acc}} = \dot{m} \mathcal{M} L_{\text{Edd}}, \quad (2)$$

with  $\dot{m}$  the mass accretion rate normalized to the Eddington one and  $\mathcal{M} = M_{\text{BH}}/M_{\odot}$ , where  $M_{\text{BH}}$  is the mass of the black hole; one can calculate the magnetic field energy density at position  $z$ :

$$U_{\text{B}} \propto \eta_{\text{b}} \dot{m} \mathcal{M}^{-1}, \quad (3)$$

where  $\eta_{\text{b}}$  is a proportionality constant. We assume for the external photon field that is related to photons that are scattered on accretion disk wind particles [10] and thus the external photon field density  $U_{\text{ext}}$  in the jet frame has the form:

$$U_{\text{ext}} = \Gamma^2 U_{\text{sc}} \propto \Gamma^2 \epsilon \dot{m}^{\alpha+1} \mathcal{M}^{-1} \quad (\alpha = 1 \text{ for } \dot{m} \geq 0.1 \text{ and } \alpha = 2 \text{ for } \dot{m} < 0.1), \quad (4)$$

where  $\epsilon$  is the efficiency of the conversion of the accreting mass into radiation and  $\Gamma$  is the bulk Lorentz factor of the source. We have assumed that the disk emits like a black body characterized by a temperature  $T_{\text{disk}}$  to estimate the spectrum of the scattered photons. As we pointed out in [10], all input parameters required for the calculation of the spectrum are scaled with  $\dot{m}$  and  $\mathcal{M}$ . Using the above definitions for the physical properties of the source, we obtain the Blazar SED, by solving the coupled integro-differential kinetic equations of electrons and photons as described in [2]. We emphasize that according to relations 3,4, the basic parameters of the system of equations depend only on the mass accretion rate,  $\dot{m}$ .

Electrons accelerate with a characteristic timescale that depends on their energy and magnetic field strength. In the case of the first-order Fermi acceleration, we have

$$t_{\text{accFI}} \geq 6 \left( \frac{c}{u_s} \right)^2 \frac{\lambda}{c} \approx 6 \frac{r_g c}{u_s^2}, \quad (5)$$

where  $r_g = \frac{\gamma m c^2}{e B}$ . The characteristic timescale of the problem is the initial crossing time of the source,  $t_{\text{cr}} = \frac{R_0}{c}$ .

We developed a numerical code [7], based on [2] to calculate the temporal evolution of the electrons and photons distribution function. This code solves two sets of integro-differential equations, each describing the losses/sinks ( $\mathcal{L}$ ) and acceleration of relativistic electrons) and photons in the emitting region. In the current study, we assume a characteristic acceleration timescale; thus, we don't have a pre-accelerated electron distribution. The kinetic equation of electrons reads:

$$\frac{\partial N(\gamma, t)}{\partial t} + \frac{N(\gamma, t)}{t_{esc}(\gamma)} + \frac{\partial}{\partial \gamma} \left[ \frac{\gamma}{t_{acc}(\gamma)} N(\gamma, t) \right] = \sum \mathcal{L}_i N(\gamma, t)$$

$$\sum \mathcal{L}_i = \frac{\partial}{\partial \gamma} [A_{syn}(\gamma, t) + A_{ICS}(\gamma, t) + A_{exp}(\gamma, t)]$$

where the terms  $A_{syn}$ ,  $A_{ICS}$ ,  $A_{exp}$  are the loss rates for synchrotron emission, inverse Compton scattering, and adiabatic expansion respectively.

In the case of particle re-acceleration episode in the distance  $z = z_0 + u_{exp}t_0$  from the central engine, motivated by the shape of the photon pulses, we assume for the electrons number an injection form:

$$q_e = q_{e0} \left( 1 + \frac{\alpha w^2}{4(t - t_0)^2 + w^2} \right). \quad (6)$$

As a zero-order approximation, the characteristic acceleration timescale remains constant; in the general description of the problem,  $t_{acc}$  should depend on the magnetic field strength.

### 3. Results

In [11], we presented a two-zone model: particles accelerate in a zone closer to the central engine, then escape to a larger volume further away and cool due to synchrotron and inverse Compton losses. Assuming that many plasma blobs are produced and evolve in each region (acceleration and radiation), we create a multi-zone emission model, Fig. 1. Here, we will focus on the acceleration region and study the photons' emission via a re-acceleration particle episode in the acceleration zone.

In Figure 2, we present the dependence of a flare on various physical parameters within the context of our study. We consider a particle re-acceleration episode where Equation 6 is employed, with  $\alpha = 0.5$  and  $w = 2t_{cr}$ . Our results for  $t_0 = 50$  provide insights into the underlying physical mechanisms and the effects of radiative cooling and adiabatic expansion. The other parameters are as follows:  $B_0 = 1.6$  Gauss,  $u_{exp} = 0.1c$ ,  $R_0 = 10^{16}$  cm, and the magnetic field strength decreases linearly with time. This particle re-acceleration episode predominantly occurs in an almost optically thick region for radio photons. For  $\gamma$ -ray photons, Inverse Compton scattering, particularly synchrotron self-Compton, is the primary mechanism, except in the last panel, where we study the contribution of an external photon field. Synchrotron radiation produces radio photons, although synchrotron self-absorption is also present. In Figure 2, the left side refers to  $\gamma$ -ray emission, while the right side corresponds to radio emission. The first row displays the dependence of the flare on the initial magnetic field strength. The shape and symmetry of the pulse remain unchanged in the  $\gamma$ -ray regime; only the luminosity varies, which is related to the luminosity of the synchrotron photons acting as targets for the relativistic electrons. In the case of radio

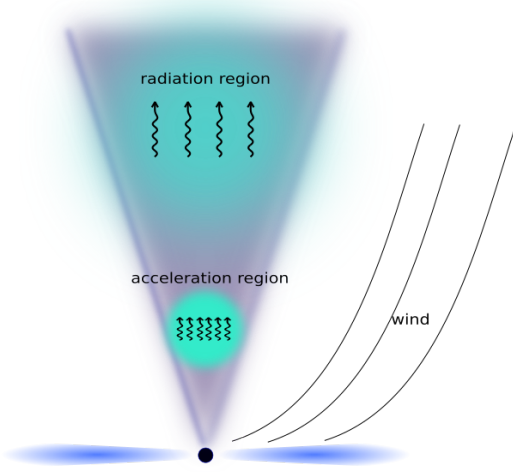


**Figure 1:** Sketch of the multi-zone model. Particles accelerate and radiate in the acceleration region (cyan), where blobs of plasma are produced and expand. In this region, the magnetic energy density is larger than the external's photon energy density ( $U_B > U_{ext}$ ). While a fraction of the accelerated particles escape into a larger expanding volume (light blue), where they cool and radiate ( $U_B < U_{ext}$ ) in the case of FSRQs objects.

photons, lower magnetic field values lead to higher luminosity flares due to the dependence of synchrotron self-absorption on the magnetic field strength. Moving to the second row, we examine the expansion velocity, which changes the pulse symmetry. The episode occurs at the same  $t_0$  for all cases, implying that for higher values of  $u_{exp}$ , the flare is produced closer to the central engine, where radiative cooling plays a more significant role. In the case of radio photons, when  $u_{exp}$  is significantly larger, the radius increases faster, resulting in a slightly more luminous flare compared to the bulk emission. In the third panel, we investigate the contribution of the acceleration timescale  $t_{acc}$ , which affects the shape of the pulse. Lower values of  $t_{acc}$  indicate that particles do not gain energy rapidly enough, and adiabatic losses become more prominent. Additionally, in the case of radio photons, a dip is observed at higher values of  $t_{acc}$  due to spectral changes. Moving to the fourth panel, we vary the initial electron number ( $N_2 > N_1$ ), revealing an interesting observation. We observe a dip in the  $\gamma$ -ray regime, which is associated with the cutoff in the spectral energy distribution. However, this behavior is not observed in radio photons. In the radio band, the electron distribution's role becomes apparent in synchrotron self-absorption, where smaller values result in the source becoming optically thin compared to other values. Finally, in the last row, the contribution of the external photon field is examined, yielding more complex results. For radio photons, the emission is solely affected by changes in the maximum electron Lorentz factor. In the case of  $\gamma$ -rays, the presented luminosity cannot be straightforwardly explained due to the cutoff, necessitating an analysis of the spectral energy distribution.

In Figure 3, we present a comparison of results for two different time instances:  $t_0=50$  and  $500 t_{cr}$ . The first case corresponds to the optically thin region, while the second represents the optically thick region. The remaining parameters have the same values as in Figure 2. Subfigures (a) and (b) display the Spectral Energy Distributions. In subfigure (a), the flare is energetically significant due to radiation cooling, while in the later flare (subfigure (b)), the energy level is comparatively lower. A comparison between plots (c) and (d) reveals that at  $t_0 = 50 t_{cr}$ , the flares exhibit greater symmetry due to the strong cooling effect. On the other hand, for  $t_0 = 500 t_{cr}$ , the flares are more extended due to adiabatic losses. Furthermore, when comparing plot (c) with plot (d), it can be observed that gamma rays decrease more rapidly in plot (d) due to the production of

second-generation synchrotron self-Compton photons. In subfigures (e) and (f), we investigate the differences in specific luminosities across the radio, X-ray, and  $\gamma$ -ray bands. These plots provide insights into the spectral index variation during flaring activity. Comparing plot (e) with plot (f), it becomes apparent that adiabatic losses significantly influence the duration and shape of spectral variability.

#### 4. Summary

In conclusion, the preliminary results obtained from our study provide valuable insights into a multi-zone emission blazar model that incorporates particle acceleration. These findings highlight the importance of considering factors such as particle acceleration timescale, the contribution of the external photon field, and the correlation across different wavelengths during flaring activity. While our numerical code has proven to be a powerful tool for investigating the emission, further research is warranted to delve deeper into these aspects and to compare our model predictions with observational data. Such endeavors will enhance our understanding of the underlying physical mechanisms driving the observed phenomena and contribute to advancing blazar studies.

**Acknowledgments:** S.B. would like to thank Apostolos Mastichiadis and Demosthenes Kazanas for the fruitful discussions and guidance.

#### References

- [1] J.G. Kirk, F.M. Rieger and A. Mastichiadis *A&A* **333** (1998) 452 [[astro-ph/9801265](#)].
- [2] A. Mastichiadis and J.G. Kirk *A&A* **295** (1995) 613.
- [3] Dimitrakoudis, S., Mastichiadis, A., Protheroe, R. J. and Reimer, A. *A&A* **546** (2012) A120.
- [4] A.P. Marscher, S.G. Jorstad, F.D. D’Arcangelo, P.S. Smith, G.G. Williams, V.M. Larionov et al. *Nature* **452** (2008) 966.
- [5] H. van der Laan *Nature* **211** (1966) 1131.
- [6] S. Boula, M. Petropoulou and A. Mastichiadis *Galaxies* **7** (2018) 3 [[1901.08793](#)].
- [7] S. Boula and A. Mastichiadis *A&A* **657** (2022) A20 [[2110.05325](#)].
- [8] A. Tramacere, V. Sliusar, R. Walter, J. Jurysek and M. Balbo *A&A* **658** (2022) A173 [[2112.03941](#)].
- [9] M. Zacharias *A&A* **669** (2023) A151 [[2211.12283](#)].
- [10] S. Boula, D. Kazanas and A. Mastichiadis *MNRAS* **482** (2019) L80 [[1810.01796](#)].
- [11] S. Boula, A. Mastichiadis and D. Kazanas in *37th International Cosmic Ray Conference*, p. 678, Mar., 2022, DOI [[2108.02467](#)].

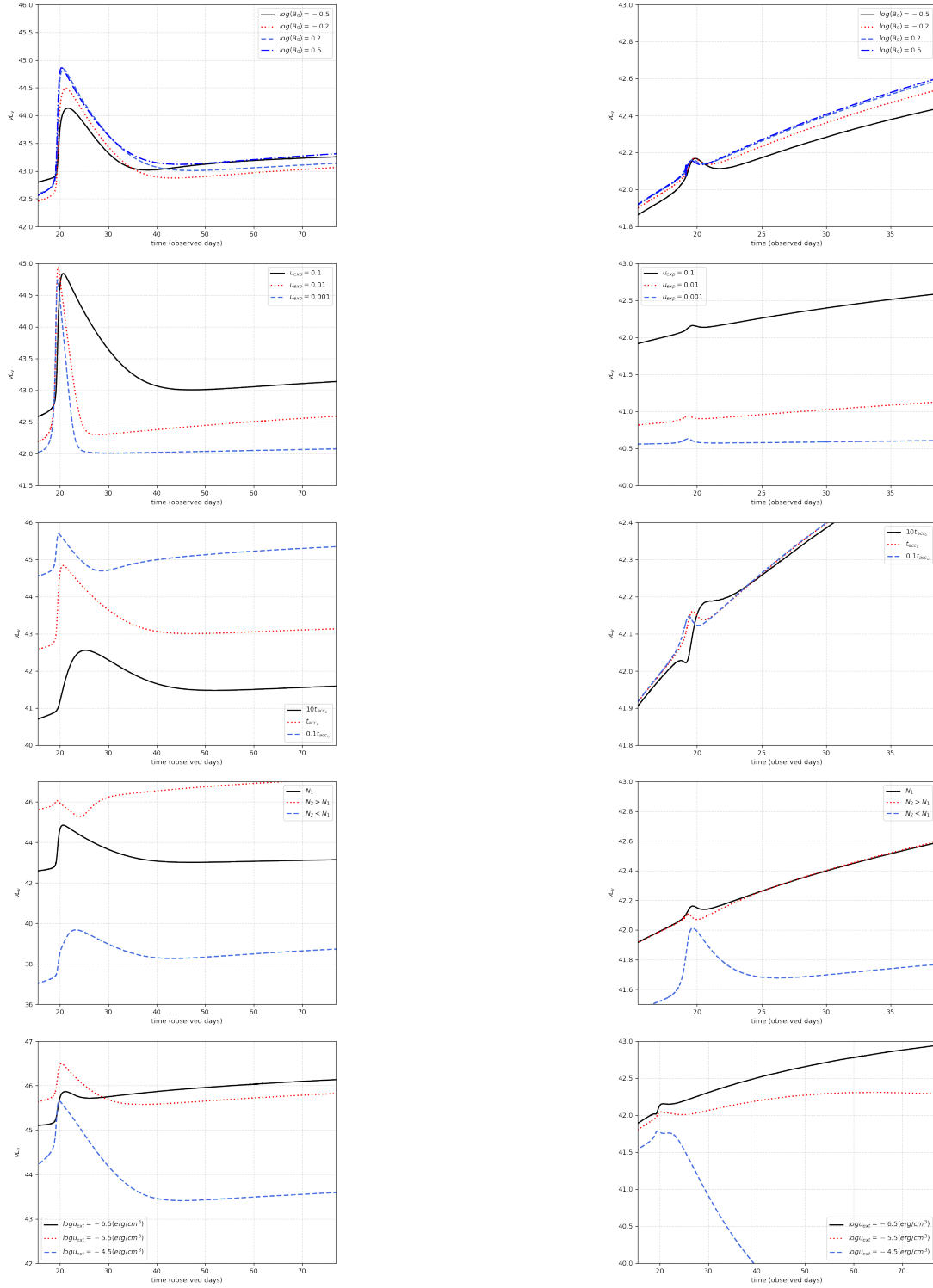
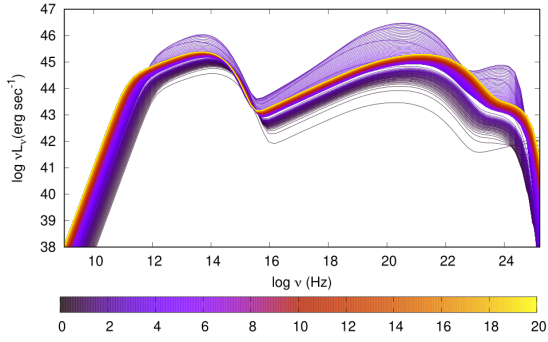
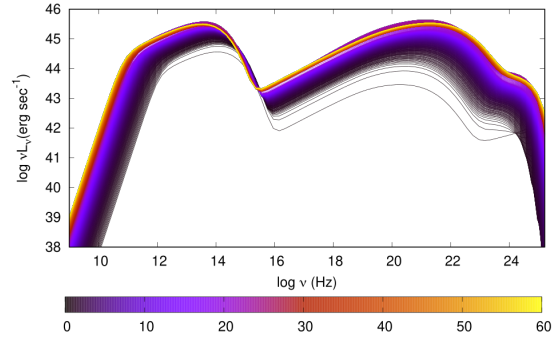


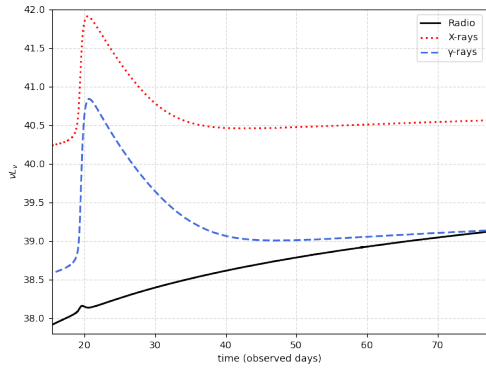
**Figure 2:** The dependence of  $\gamma$ -ray (left plot) and radio (right plot) flares on the physical quantities.



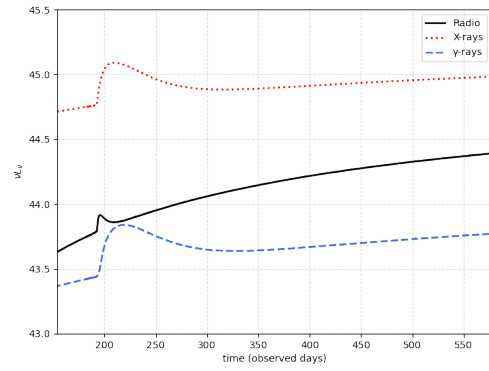
(a) The evolution of the Spectrum Energy Distribution when the re-acceleration episode happens at  $t_O = 50t_{cr}$ . The time unit is the observed days.



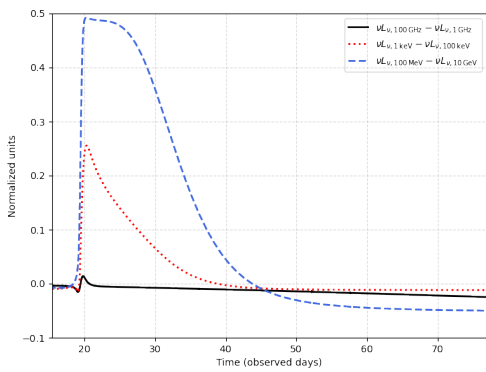
(b) The evolution of the Spectrum Energy Distribution when the re-acceleration episode happens at  $t_O = 500t_{cr}$ . The time unit is the observed days.



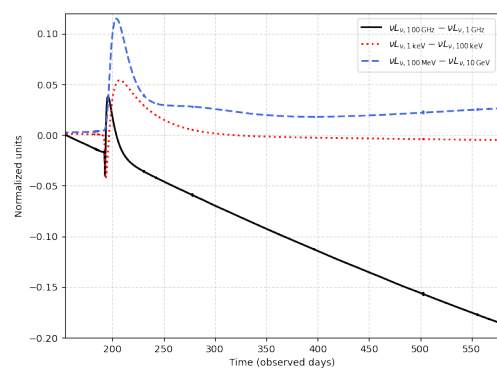
(c) A flare in the initial stages of blob's evolution. There is small time lag between the different energies. Flare is more symmetric due to the strong cooling from radiative losses.



(d) A flare in the initial stages of the blob's evolution. There is a small time lag between the different energies. Flare is more extended due to adiabatic losses.



(e) Differences between specific radio, X-ray, and  $\gamma$ -ray luminosities for a re-acceleration episode in earlier stages.



(f) Differences between specific radio, X-ray, and  $\gamma$ -ray luminosities for a re-acceleration episode in later stages.

**Figure 3:** Photons emission dependence on the time of particle re-acceleration episode.